Identifying the wavenumber for the inverse Helmholtz problem using an enriched finite element formulation

Jinhui Jiang[1], M Shadi Mohamed[2,*], Mohammed Seaid[3], Hongqiu Li[4]

[1] *State Key Laboratory of Mechanics and Control of Mechanical Structures, Nanjing University of Aeronautics and Astronautics, Nanjing, 210016, China*

[2] *School of Energy, Geoscience, Infrastructure and Society, Heriot-Watt University, Edinburgh EH14 4AS, UK*

[3] *School of Engineering and Computing Sciences, University of Durham, UK*

[4] *Jinling Institute of Technology, Mechatronic Engineering College, Nanjing, 211169, China*

Abstract

We investigate the inverse problem of identifying the wavenumber for the Helmholtz equation. The problem solution is based on measurements taken at few points from inside the computational domain or on its boundary. A novel iterative approach is proposed based on coupling the secant and the descent methods with the partition of unity method. Starting from an initial guess for the unknown wavenumber the forward problem is solved using the partition of unity method. Then the secant/descent methods are used to improve the initial guess by minimising a predefined objective function based on the difference between the solution and a set of data points. In the next round of iterations the improved wavenumber estimate is used for the forward problem solution and the partition of unity approximation is improved by adding more enrichment functions. The iterative process is terminated when the objective function has converged and a set of two predefined tolerances are met. To evaluate the estimate accuracy we propose to utilise extra data points. To validate the approach and test its efficiency two wave applications with known analytical solutions are studied. The results show that the proposed approach can achieve high accuracy for the studied applications even when the considered data is contaminated with noise. Despite the clear advantages that were previously shown in the literature for solving the forward Helmholtz problem, this work presents a first attempt to solve the inverse Helmholtz problem with an enriched finite element approach.

Keywords. Finite element method; Partition of unity method; Helmholtz equation; Acoustic wave; Inverse problem; Wavenumber identification.

1 Introduction

The inverse problem of the Helmholtz equation is relevant to numerous engineering applications, e.g., medical and subsurface imaging, microwave, radar, sonar and laser. The problem can be classified into two main classes [1, 2]: the first one looks into recovering the unknown boundary conditions based on measuring the wave field at a number of points inside or on the boundaries of the considered domain [3–5]. The second class is to identify the subsurface material properties or any internal sources based on similar measurements [2, 6–8]. The work in this paper belongs to the latter class where we aim at identifying the wavenumber based on measuring the wave field inside the domain or on its boundaries. This problem is primarily motivated by medical applications where it is desirable to use

*Coresponding author: m.s.mohamed@hw.ac.uk

electromagnetic or acoustic wave measurements on the human body to assess an organ condition. Identifying the wavenumber can be useful to diagnose any abnormal conditions that may affect the organ.

Solutions of the inverse problem can be challenging mathematically due to the often incomplete knowledge about the problem where issues such as ill-posedness and ill-conditioning are common features [1, 2, 9, 10]. Several authors have studied the uniqueness and stability of the problem [11, 12]. A number of numerical methods are often used for solving the inverse Helmholtz problem. These methods include the continuation method [13], the Fourier method [14–16] and the linear sampling method [17, 18] among others. Iterative solvers involving solution of the forward problems have also been used in the inverse problems, see for example [19, 20]. In [19], a class of iterative algorithms were combined with the finite difference method to solve the inverse Helmholtz problem. Recently, in the context of the diffusion problem, a set of problem-adapted basis functions were proposed in [20] for the multiscale finite element method to solve the problem of identifying diffusion coefficients. Obviously, in this case the accuracy of the inverse problem solution depends strongly on the solution of the forward problem as well as the accuracy of the field measurements. Two approaches are available for solving the forward problem. First, it is possible to develop analytical solutions which are highly accurate and not demanding computationally but they are only viable for simple geometries. Examples of analytical solutions of many classical wave problems can be found in [21–24]. The second approach relies on numerical methods which are often used for engineering applications and can deal with general geometries. The Finite Element Method (FEM) [20] and the Boundary Element Method [25] are among the most popular. As a rule-of-thumb and for a given problem, a discretization level of around ten nodal spaces per wavelength is necessary to achieve a reasonable engineering accuracy. This can be the case for long wave problems, i.e., the computational domain accommodates only a few waves per-direction. However, the error increases quickly if for a given problem we increase the wavenumber and retain the discretization level of ten. This behaviour is well documented in the literature and is referred to as the pollution error [26–28].

To overcome the pollution error when linear elements are used, it is necessary to increase the number of nodal spaces per-wavelength at a quadratic rate as the wavenumber increases at a linear rate [26]. Hence, the numerical methods can become computationally non-viable at higher wavenumbers. Improving the approximation properties of the numerical methods can significantly reduce the number of degrees of freedom required to achieve a given accuracy. A major improvement was possible by incorporating oscillatory functions into the approximation space using the Partition of Unity Method (PUM) [29]. It was possible to enrich the finite elements with plane waves, hence, reduce the number of degrees of freedom without compromising on the solution accuracy [30, 31]. Similar improvement was also achieved using Bessel functions [32]. The new elements are used for solving acoustic [33], elastic [34] and electro-magnetic waves [35, 36]. It was also used to solve problems in layered media [30], heterogeneous media [37] and poroelastic media [38]. Similarly to the frequency-domain, the enriched elements were also used for time-domain wave and heat transfer problems [35,39–42]. Adding enrichment functions to the finite element approximation space can also be achieved with discontinuous elements. Examples include the discontinuous enrichment method [43, 44], the ultra weak variational formulation [45,46] and other discontinuous Galerkin methods [47–49]. A recent review of the literature about using enriched elements for the Helmholtz problem can be found in [50]. This growing body of literature shows that the enriched finite element can lead to a significant reduction in the computational efforts in terms of memory and CPU time, compared to the standard finite element method.

Despite the high efficiency of the enriched methods in solving the forward problem, these methods have not been yet utilised for solving the inverse problem. This has been the case so far although the potential impact of these methods on the inverse problem can be a lot more significant compared to the forward problem. The inverse problem often involves lengthy iterative procedures with each iteration being in some cases equivalent to solving a full-length forward problem. Therefore reducing the computational costs can be crucial for solving the inverse problem. Furthermore, an iterative procedure

starts with a certain estimate for the wavenumber which will then be improved as the iterations progress. If an improved wavenumber estimate is higher then it may become necessary to refine the finite element mesh. This refinement process can be eliminated with the enrichment approach. In this work we propose solving the inverse problem by coupling the secant and descent methods with the PUM. To validate the proposed approach we consider problems with known analytical solutions. Despite the clear advantages, an extensive literature review suggests that this work is the first use of an enriched numerical approach for solving the inverse Helmholtz problem. It is also important to mention that limited literature is currently available on wavenumber identification for the Helmholtz equation, where we also make a contribution. The rest of this paper is organized as follows. First, we present the inverse method to estimate the wavenumber based on the PUM and secant and descant methods in Section 2 and section 3. Section 4 provides two numerical experiments to test the effectiveness and accuracy of the proposed approach where wave propagation and scattering are considered. We finish in section 5 with some concluding remarks.

2 PUM formulation for estimating the wavenumber

In the current study, we assume a time-harmonic wave propagation i.e. $\phi = ue^{\mathrm{i}\omega t}$ where ϕ is the time-dependent wave potential, ω the frequency, t time and i defined by $\mathrm{i}=\sqrt{-1}$. The wave equation can then be reduced to the Helmholtz equation which in a two-dimensional domain $\Omega \subset \mathbb{R}^2$ can be written as

$$\Delta u + k^2 u = 0, \qquad \text{in } \Omega. \tag{2.1}$$

Here, $u(\mathbf{x})$ is the time-independent wave field while Δ is the Laplace operator, $(k = \frac{\omega}{c})$ the wavenumber and c the wave speed. For practical reasons we need to impose some artificial boundary Γ so that the computational domain Ω is finite. To avoid introducing errors through the artificial boundary we choose to impose the analytical solution of any considered problem, on Γ using a Robin type boundary condition

$$\frac{\partial u}{\partial \mathbf{n}} + \mathrm{i}ku = g, \qquad \text{on } \Gamma, \tag{2.2}$$

where $\mathbf{n}$ is the outward unit normal on Γ and $g(\mathbf{x})$ is a source term defined based on the imposed analytical solution.

In this paper we are interested in identifying the unknown wavenumber k based on known values of $u(\mathbf{x})$ at a given set of points $\mathbf{x} \in \Omega$. Hence, a relationship between the wavenumber and the measured field should be established. To this end we will derive this relation based on the weak formulation of the forward problem (2.1)-(2.2). As mentioned above we adopt an enriched finite element formulation which is more efficient than the standard formulation. Several options are possible, however, choosing a discontinuous formulation can add more complexity for solving the inverse problem where a nonlinear problem must be solved in order to identify the wavenumber in term of the field values. Therefore we prefer the continuous formulation of the PUM.

Starting from the boundary value problem defined by the equations (2.1)-(2.2), then using a weighted residual scheme, the governing finite element integral equations for the problem becomes

$$\int_\Omega w\Big(\Delta u + k^2 u\Big) d\Omega = 0, \tag{2.3}$$

$$\oint_\Gamma w\Big(\frac{\partial u}{\partial \mathbf{n}} + \mathrm{i}ku\Big) d\Gamma = \oint_\Gamma w g d\Gamma, \tag{2.4}$$

where $w(\mathbf{x})$ is the weighting function. Applying Green's theorem to equation (2.3) we obtain

$$\int_\Omega \Big(- \nabla w \cdot \nabla u + k^2 w u\Big) d\Omega + \oint_\Gamma w \frac{\partial u}{\partial \mathbf{n}} d\Gamma = 0, \tag{2.5}$$

and substituting the boundary condition we arrive at the following weak formulation

$$\int_\Omega \Big(\nabla w \cdot \nabla u - k^2 wu\Big) d\Omega + \mathrm{i}k \oint_\Gamma wu d\Gamma = \oint_\Gamma w g d\Gamma. \tag{2.6}$$

Using the PUM, the computational domain Ω is subdivided into elements Ω_e with n-nodes for each element so that the solution $u(\mathbf{x})$ at $\mathbf{x} = (x, y) \in \Omega_e$ can be approximated in term of the values d_i^e at the element nodes

$$u(\mathbf{x}) \approx u^e(\mathbf{x}) = \sum_{i=1}^{n} \sum_{j=1}^{m} N_i^e(\mathbf{x}) \varphi_{i,j}^e(\mathbf{x}) d_{(i-1)m+j}^e, \tag{2.7}$$

where $N_i^e(\mathbf{x})$ is the conventional polynomial shape function of the finite element Ω_e at the node i, $\varphi_{i,j}^e(\mathbf{x})$ is the jth order partition of unity enrichment function also at node i and m is the total number of enrichment functions. Note that for wave problems often oscillatory functions are chosen to enrich the finite element approximation space. Similar to above we can also write $w(\mathbf{x})$ in terms of the values r_i^e as

$$w(\mathbf{x}) = w^e(\mathbf{x}) = \sum_{i=1}^{n} \sum_{j=1}^{m} N_i^e(\mathbf{x}) \varphi_{i,j}^e(\mathbf{x}) r_{(i-1)m+j}^e. \tag{2.8}$$

Hence, equation (2.6) becomes

$$\sum_{e=1}^{N_e} \left(\int_{\Omega_e} \nabla w^e \cdot \nabla u^e d\Omega_e - k^2 \int_{\Omega_e} w^e u^e d\Omega_e + \mathrm{i}k \oint_{\Gamma^e} w^e u^e d\Gamma_e - \oint_{\Gamma^e} w^e g d\Gamma_e \right) = 0. \tag{2.9}$$

where N_e is the total number of elements. For convenience the vectors $\mathbf{N}^e, \mathbf{d}^e$ and $\mathbf{r}^e$ are defined for each element Ω_e as

$$\begin{aligned}
\mathbf{N}^e &= \Big\{ N_1\varphi_1, N_1\varphi_2, ...N_1\varphi_m, N_2\varphi_1, ..., N_n\varphi_m \Big\}^\top, \\
\mathbf{d}^e &= \{ d_1^e, d_2^e, ...d_m^e, d_{m+1}^e, ..., d_{nm}^e \}^\top, \\
\mathbf{r}^e &= \{ r_1^e, r_2^e, ...r_m^e, r_{m+1}^e, ..., r_{nm}^e \}^\top.
\end{aligned}$$

The entries $d_{(i-1)m+j}^e$ and $r_{(i-1)m+j}^e$ are associated with the node i and the jth order enrichment function for the element Ω_e. The global nodal vector for all the nodes in the domain Ω is denoted by $\mathbf{d}$ while for the weighting functions by $\mathbf{r}$. We define the rectangular matrix $\mathbf{L}^e$ made of entries equal to ones or zeros so that we can write a relationship between the element level vector $\mathbf{d}^e$ and the global level vector $\mathbf{d}$ as

$$\mathbf{d}^e = \mathbf{L}^e \mathbf{d}.$$

For any element we can also write

$$(\mathbf{r}^e)^\top = \mathbf{r}^\top (\mathbf{L}^e)^\top.$$

Then, the gradient of $u^e(\mathbf{x})$ and $w^e(\mathbf{x})$ can be computed by

$$\nabla u^e = \nabla \mathbf{N}^e \mathbf{L}^e \mathbf{d} = \mathbf{B}^e \mathbf{L}^e \mathbf{d},$$

$$(\nabla w^e)^\top = \mathbf{r}^\top (\mathbf{L}^e)^\top (\nabla \mathbf{N}^e)^\top = \mathbf{r}^\top (\mathbf{L}^e)^\top (\mathbf{B}^e)^\top.$$

The weak formulation can be rewritten in matrix form as

$$\mathbf{r}^\top \left(\sum_{e=1}^{N_e} (\mathbf{L}^e)^\top \left(\left(\int_{\Omega_e} (\mathbf{B}^e)^\top \mathbf{B}^e d\Omega - k^2 \int_{\Omega_e} (\mathbf{N}^e)^\top \mathbf{N}^e d\Omega + \mathrm{i}k \oint_{\Gamma^e} (\mathbf{N}^e)^\top \mathbf{N}^e d\Gamma \right) \mathbf{L}^e \mathbf{d} - \oint_{\Gamma^e} (\mathbf{N}^e)^\top g d\Gamma \right) \right) = \mathbf{0}.$$

Note that the above equation shows the contribution made by different integrals to the element matrix

$$\mathbf{K}^e = \underbrace{\int_{\Omega_e} (\mathbf{B}^e)^\top \mathbf{B}^e d\Omega}_{\mathbf{K}_k^e} - k^2 \underbrace{\int_{\Omega_e} (\mathbf{N}^e)^\top \mathbf{N}^e d\Omega}_{\mathbf{K}_m^e} + \mathrm{i}k \underbrace{\oint_{\Gamma^e} (\mathbf{N}^e)^\top \mathbf{N}^e d\Gamma}_{\mathbf{K}_c^e}. \tag{2.10}$$

A high order quadrature scheme is usually needed to evaluate the above integrals as they involve oscillatory functions. After evaluating the integrals the following linear system of equations is achieved

$$\underbrace{\left[\sum_{e=1}^{N_e} (\mathbf{L}^e)^\top \mathbf{K}^e \mathbf{L}^e\right]}_{\mathbf{K}} \mathbf{d} - \underbrace{\left\{\sum_{e=1}^{N_e} (\mathbf{L}^e)^\top \mathbf{f}^e\right\}}_{\mathbf{f}} = 0.$$

To find the relation between the wavenumber and the measured field, we find $\mathbf{K}^+$ which is the Moore–Penrose pseudo inverse of $\mathbf{K}$

$$\mathbf{d} = \mathbf{K}^+ \mathbf{f}.$$

Thus, from equation (2.7) the relationship between the wavenumber and the measured field at $\mathbf{x}$ can be obtained by

$$u^{\mathrm{e}}(\mathbf{x}) = \mathbf{N}^{\mathrm{e}} \mathbf{L}^{\mathrm{e}} \mathbf{d} = \mathbf{N}^{\mathrm{e}} \mathbf{L}^{\mathrm{e}} \left[\sum_{e=1}^{N_e} (\mathbf{L}^e)^\top \left(\mathbf{K}_k^e - k^2 \mathbf{K}_m^e + \mathrm{i}k \mathbf{K}_c^e\right) \mathbf{L}^e\right]^+ \mathbf{f}, \tag{2.11}$$

where $\mathbf{x} \in \Omega_{\mathrm{e}}$. In general this relation is severely nonlinear because $\mathbf{N}^e$, $\mathbf{f}$ and $\mathbf{K}^+$ can all be dependent on the wavenumber. Hence, no analytical expression for the wavenumber can be obtained with respect to the wave field and an iterative solution strategy must be developed to solve the inverse problem of identifying k in terms of the solution $u^{\mathrm{e}}(\mathbf{x})$.

3 Solution of the inverse problem

To solve the nonlinear equation (2.11) we propose an iterative algorithm which estimates the wavenumber by minimizing an objective function. First, we collect the data obtained from an experiment or a numerical/analytical simulation of the wave field. Assuming that the number of the data points is Q, we collect them in pairs as:

$$\Big[\mathbf{x}_q, u_q^*(\mathbf{x}_q)\Big], \qquad\qquad q = 1, 2, ..., Q,$$

where $\mathbf{x}_q$ is the location of the qth data point and $u_q^*(\mathbf{x}_q)$ is the field measured at this point. The data points can either be picked up from inside the domain or on the domain boundary. In theory one data point ($Q = 1$) is enough to have an estimate for the wavenumber. However, in practice and depending on the completeness/accuracy of the collected data it may be necessary to use more data points to have confidence in the estimation and to make sure the algorithm converges to the correct solution. Based on the physical knowledge about the problem under consideration, it will be possible to have a reasonable initial guess for the wavenumber. Often in real-world applications the initial information about the domain material properties can provide this physical knowledge which will also give confidence in the converged wavenumber estimate. Using the estimate of the wavenumber $\hat{k}$ we solve the forward problem following the approach described in the previous section. Next, we define the objective function based on the following residual

$$f_q(k) = u_q^*(\mathbf{x}_q) - \hat{u}_q(\mathbf{x}_q, \hat{k}), \tag{3.1}$$

which represents the difference between the numerical solution of the field $\hat{u}_q(\mathbf{x}_q, \hat{k})$ and the measured field $u_q^*(\mathbf{x}_q)$ at the qth data point. The numerical prediction is obtained through the relation (2.11) and using the estimated wavenumber $\hat{k}$

$$\hat{u}_q(\mathbf{x}_q, \hat{k}) = \hat{\mathbf{N}}^e \cdot \mathbf{L}^e \left[\sum_{e=1}^{N_e} (\mathbf{L}^e)^\top \left(\hat{\mathbf{K}}_k^e - \hat{k}^2 \hat{\mathbf{K}}_m^e + \mathrm{i}\hat{k} \hat{\mathbf{K}}_c^e \right) \mathbf{L}^e \right]^+ \hat{\mathbf{f}}. \tag{3.2}$$

In the current work we will rely on analytical solutions to evaluate $u_q^*(\mathbf{x}_q)$. This is important to accurately evaluate the error. The objective function can then be defined as:

$$\text{Minimize} \quad \vartheta(k) = \frac{1}{Q} \sum_{q=1}^{Q} \frac{|f_q(k)|}{\left|u_q^*(\mathbf{x}_q)\right|} = \frac{1}{Q} \sum_{q=1}^{Q} \frac{\left|u_q^*(\mathbf{x}_q) - \hat{u}_q(\mathbf{x}_q, \hat{k})\right|}{\left|u_q^*(\mathbf{x}_q)\right|}, \tag{3.3}$$

subject to (2.6). Note that values of the measured field can vary between numbers close to zero at some data points to numbers significantly larger than zero at others. Therefore, the objective function is defined as a relative function in order to normalise the contribution made by different data points such that no one data point dominates the value of the objective function. Clearly more data points provide more confidence in the solution. Let $l = 1, 2, ...$ be the iterative step and $\hat{k}_l$ be the iterative estimation of the wavenumber. For the purpose of the calculations in this paper we assume that the wavenumber is always a real positive number and will be reset to a positive number if a negative wavenumber is estimated. The secant method is used to update the wavenumber estimation as the method convergence to the exact root is ensured when the initial value is close to the exact root [51]. Furthermore, we also use the descent method to avoid divergence when the initial estimate $\hat{k}_0$ is far from the exact root where the method ensures the convergence also in this case. The updated wavenumber can then be written as

$$\hat{k}_{l+1} = \hat{k}_l - \mu f_q(\hat{k}_l) \frac{\hat{k}_l - \hat{k}_{l-1}}{f_q(\hat{k}_l) - f_q(\hat{k}_{l-1})}, \tag{3.4}$$

where μ should be within the range $0 < \mu \leq 1$ in order to minimize the residual $f_q(k)$ such that

$$\left| f_q(\hat{k}_{l+1}) \right| < \left| f_q(\hat{k}_l) \right|. \tag{3.5}$$

The value of μ is determined by initializing it with 1 and then halving its value until satisfying the condition (3.5). To estimate the wavenumber we propose a two-stage iterative algorithm which is shown in Figure 3.1. The first stage is to determine an appropriate number of enrichment functions m which is needed for the PUM approximation. The second stage is to estimate the wavenumber $\hat{k}^l, l = 1, 2, ...$ for every data point based on the secant and descent methods. The stopping criterion for the first stage is

$$\vartheta(k) \leq \varepsilon_a,$$

while for the second stage the stopping criterion is

$$\min\left(|\hat{k}_{l+1} - \hat{k}_l|, |f_q(\hat{k}_l)| \right) \leq \varepsilon_b,$$

where ε_a and ε_b are predefined tolerances. It should be stressed that these tolerances are both correlated to the quality of the measured data for the problem under study. Using small values for the tolerances with contaminated data may not improve the accuracy of the estimate but it can lead to unnecessary increase in the number of iterations. However, in the current work, we consider the same tolerances for clean and contaminated data only for comparison purposes. For multiple data points multiple wavenumber estimates are found $\hat{k}^q$. In this case the estimate which leads to the minimum

value of $\vartheta(k)$, is considered to be the optimum estimate $\hat{k}_{opt}$ and it is taken forward to the next round of iterations.

It should be stressed that unlike the FEM, the PUM can retain the same mesh and only update the enrichment functions. But it is important to have a balance between the number of enrichment functions and the wavenumber [52]. The number m must be high enough to find an appropriate approximation but should not be too high in order to avoid an ill-conditioned linear system of equations. Furthermore, using an unnecessary high numbers m will increase the computation cost without improving the computation accuracy [31]. Needless to mention that previous works on enriched finite element methods for the Helmholtz equation suggest that the relation between the wavenumber and the number of enriching plane waves has to ensure that the number of degrees of freedom per wavelength is around two. This can be found in the results reported in [28, 31, 33] among others.

In this work a set of plane waves evenly spaced around a unit circle are used to enrich the finite element solution space

$$\varphi_j(\mathbf{x}) = \exp\left(\mathrm{i}\hat{k}_l\left(x\cos\left(\frac{2\pi j}{m}\right) + y\sin\left(\frac{2\pi j}{m}\right)\right)\right).$$

For the plane waves, wavenumber is updated at each iteration to match the wavenumber estimated at this iteration.

Finally, to evaluate the error in approximating the wavenumber we use two methods:

(i) In this work we use the exact wavenumber k in order to validate the approach

$$\xi_1 = \frac{\left|\hat{k} - k\right|}{k} \times 100\%. \tag{3.6}$$

(ii) In the general case where the exact wavenumber is unknown, we propose utilizing additional data points $U_p(\mathbf{x}_p)$ to verify the solution where $p = 1, 2, \ldots, P$ and P is the total number of the verification points. The estimated wavenumber is then used to evaluate the field at the same points $\hat{u}_p(\mathbf{x}_p)$. The field value at the points $U_p(\mathbf{x}_p)$ are compared to the calculated values $\hat{u}_p(\mathbf{x}_p, \hat{k})$

$$\xi_2 = \frac{1}{P}\sum_{s=1}^{P} \frac{\left|\hat{u}_p(\mathbf{x}_p, \hat{k}) - U_p(\mathbf{x}_p)\right|}{|U_p(\mathbf{x}_p)|} \times 100\%. \tag{3.7}$$

Both methods can provide useful evaluation for the error in the approximation. However, selecting a data point where the field value is very close to zero may lead to unrealistically large errors in the second method. Also here using more data points improve the error evaluation with equation (3.7).

4 Numerical results

In this section, the proposed inverse method is studied using two numerical tests. In both tests the exact solution and the wavenumber are known so that an accurate identification of the error is possible. In the first example a plane wave and in the second the scattering of a plane wave by a rigid circular cylinder, are considered. In both tests two random points are utilised to identify the wavenumber while a third point is used to verify the results.

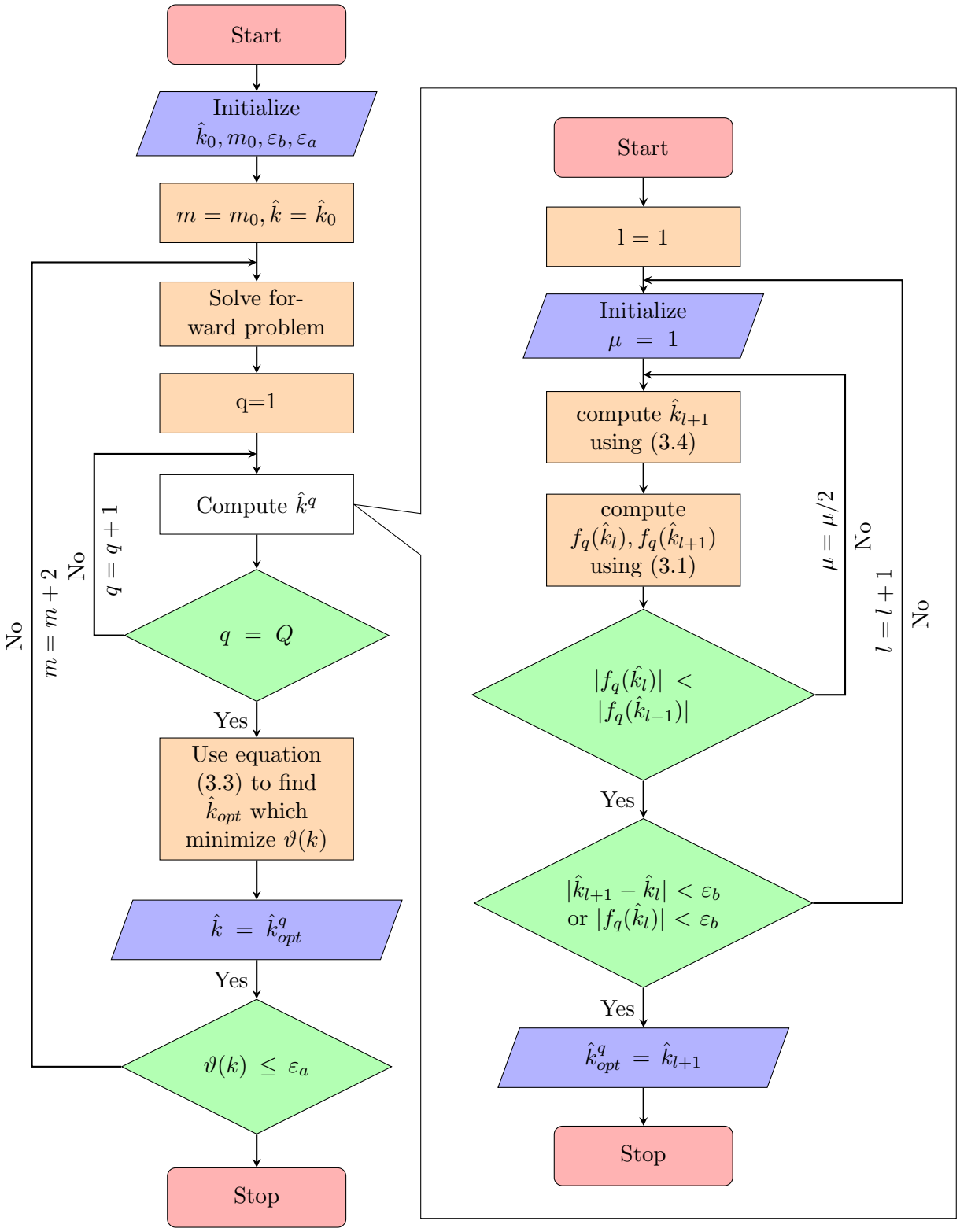

Figure 3.1: Flowchart for the iterative procedure used in our inverse solution.

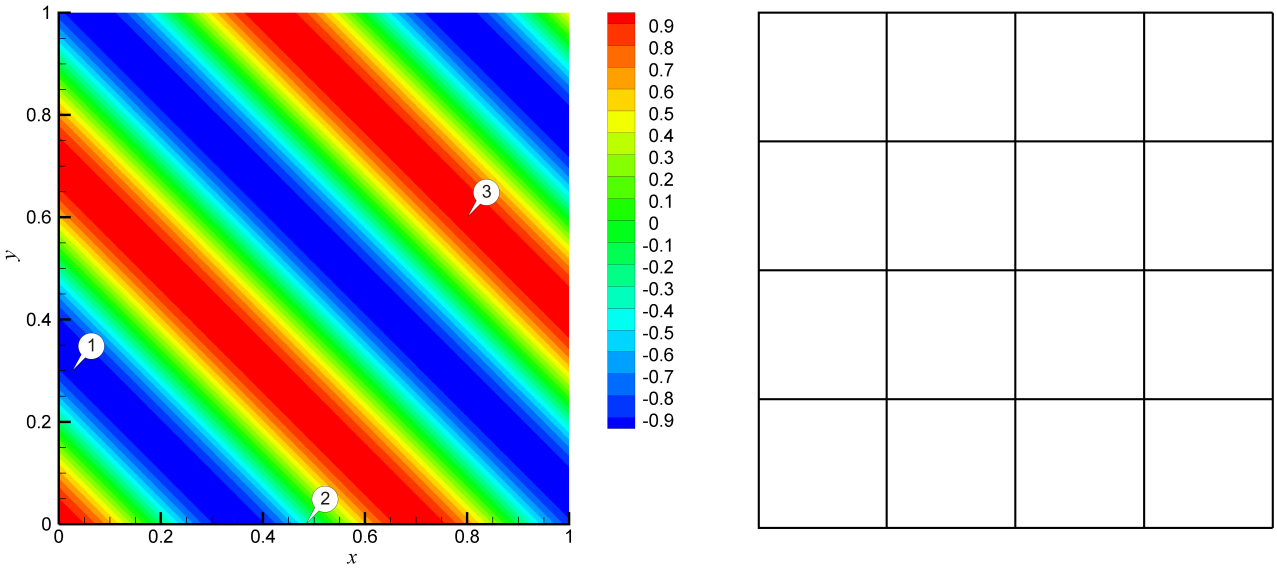

Figure 4.1: Plane wave propagation: Real part of the analytical expression for $\alpha = \frac{\pi}{4}, k = 4\pi$ (left) and the considered mesh (right). The data is measured at the points P1(0.02,0.3), P2(0.48,0.00) and P3(0.8, 0.6) indicated in the figure.

4.1 Plane wave propagation

For a plane wave propagation in a homogeneous media, the exact wave field can be expressed as

$$u_{\text{ex}} = e^{\mathrm{i}k(x\cos\alpha + y\sin\alpha)}, \tag{4.1}$$

with α being the propagation angle. We consider a squared computational domain defined by $\Omega = [0,1] \times [0,1]$ with the analytical solution imposed on the domain boundaries. For this test example the following parameters are taken $k = 4\pi$ and $\alpha = \frac{\pi}{4}$. The wave field is evaluated using expression (4.1) at three random points, namely, P1(0.02,0.3), P2(0.48,0.00) and P3(0.8, 0.6). Here, P1 and P2 are data points used to estimate the wavenumber while P3 is a verification point to evaluate the error. The points are placed such that P1 is inside the domain while P2 is on the domain boundary. It should be noted that any other points might also be used without restrictions on the points choice. The proposed algorithm may also estimate the wavenumber based on a single data point. However, in this case, the convergence to the correct k cannot be ensured. Therefore, the use of more data points is recommended. To solve the problem, the domain is discretized into 4-noded bilinear elements. Figure 4.1 shows the real part of the progressive plane wave for the considered parameters alongside the used mesh. The data points are also indicated on this figure.

To solve the problem we start with an initial guess of $\hat{k}_0 = 30$ which is more than twice the actual wavenumber $k = 4\pi$. Starting with a better guess will always speed up the convergence. In real-world applications the guess will often be informed by the physical properties of the problem. We also start by enriching the solution domain with one plane wave $m_0 = 1$. Again here starting with more enrichment functions will also speed the convergence. However, in this example we want to test the algorithm convergence when starting with relatively poor initial values. The stopping tolerances are $\varepsilon_b = 10^{-5}$ and $\varepsilon_a = 10^{-5}$. As the wavenumber estimate is refined the number of enriching plane waves is also increased until the stopping tolerances are met and the minimization function has converged. The output of the solution iterations at different stages is listed in Table 4.1 for $m = 1, 2$ and 4 and Table 4.1 for $m = 6, 8$ and 10. It should be noted that the PUM with enrichment enables using much larger finite elements compared to the standard FEM. Hence, completing the required iterations is significantly faster than using the standard FEM. Furthermore, the FEM mesh is dependent on the wavenumber. Increasing the wavenumber estimate may also require remeshing the domain. The PUM

Table 4.1: Plane wave propagation: Wavenumber iterations for $m = 1, 2$ and 4.

# Itr	$m = 1$ $(\hat{k}_0 = 30)$		$m = 2$ $(\hat{k}_0 = 11.897014)$		$m = 4$ $(\hat{k}_0 = 12.426802)$	
	P1	P2	P1	P2	P1	P2
1	33.000000	33.000000	13.086716	13.086716	13.669481	13.669481
2	23.799656	29.258212	11.894196	12.521825	12.430829	12.439952
3	21.524713	28.252650	11.512766	12.380315	12.421304	12.431215
4	33.768019	29.707779	11.945903	12.423934	12.426928	12.425210
5	14.518022	29.609562	11.933054	12.429760	12.426945	12.425140
6	2.819852	29.189728	11.820275	12.426784	12.426920	12.425110
7	16.228119	29.347688	11.854205	12.426613	12.426920	12.425110
8	18.172552	29.422310	11.875060	12.426802		
9	9.499285	29.354575	11.860515	12.426802		
10	11.378076	29.352539	11.858832			
15	11.872664	29.365516	11.861914			
20	11.897829	29.365757	11.861918			
28	11.897014					
$\hat{k}^q_{opt}$	11.897014*	29.365757	11.861918	12.426802*	12.426920	12.425110*
$\vartheta(k)$	0.0668	0.3446	0.0740	0.0645	7.1959×10^{-5}	7.1847×10^{-5}

* value used for the next round of iterations.

Table 4.2: Plane wave propagation: Wavenumber iterations for $m = 6, 8$ and 10.

# Itr	$m = 6$ $(\hat{k}_0 = 12.425110)$		$m = 8$ $(\hat{k}_0 = 12.560171)$		$m = 10$ $(\hat{k}_0 = 12.566335)$	
	P1	P2	P1	P2	P1	P2
1	13.667621	13.667621	13.811634	13.811634	13.822969	13.822969
2	12.557146	12.561449	12.566460	12.566654	12.566379	12.566378
3	12.555444	12.561641	12.566330	12.566339	12.566370	12.566370
4	12.556030	12.560173	12.566320	12.566335		
5	12.556031	12.560171				
$\hat{k}^q_{opt}$	12.556031	12.560171*	12.566320	12.566335*	12.566370	12.566370
$\vartheta(k)$	5.0055×10^{-6}	4.4504×10^{-6}	1.1284×10^{-10}	1.0358×10^{-10}	3.1348×10^{-14}	3.1348×10^{-14}

* value used for the next round of iterations.

Table 4.3: Plane wave propagation: Estimation of final errors.

	Wavenumber	Solution value at P3
Actual	4π=12.5663706	0.99202140
Estimate	12.566370	0.99202132
Error	$\xi_1 = 4.8 \times 10^{-6}\%$	$\xi_2 = 8.1 \times 10^{-6}\%$

helps to avoid remeshing the domain by merely updating the wavenumber of the enrichment functions to match the estimated wavenumber $\hat{k}_l$.

The results in Table 4.1 shows that for $m = 1$ the estimated wavenumber converges to $\hat{k}_{28} = 11.897014$ at P1 after 28 iterations and to $\hat{k}_{20} = 29.365757$ at P2 after 20 iterations. However, the minimization function is smaller for the estimate based on P1 $\vartheta(\hat{k}_{28}) = 0.0668$ compared to P2 $\vartheta(\hat{k}_{20}) = 0.3446$. Hence, the improved guess for the next round of iterations is taken based on the estimate at P1 i.e. $\hat{k}_0 = \hat{k}_{28} = 11.897014$. The estimate is further improved with $m = 2$ at the second round of iterations. The converged minimum value for $\vartheta(k)$ is achieved at P2 after 9 iterations with $\hat{k}_9 = 12.426802$. The relationship between the function $\vartheta(k)$ and the accuracy of the wavenumber estimate is evident in the results where a smaller value of $\vartheta(k)$ always indicate a more accurate estimate of the wavenumber. As the number of enriching plane waves is increased and the wavenumber estimate is improved fewer iterations becomes necessary. It can be seen in Table 4.2, the estimate converges to the exact wavenumber with six digits accuracy at points P1 and P2 with $m = 10$ and the minimization function has converged to $\vartheta(\hat{k}_3) = 3.1348 \times 10^{-14}$ at both points. Table 4.3 summarizes the converged estimate of the wavenumber with the final errors obtained using equations (3.6) and (3.7). The errors in the wavenumber estimation as well as in the verification data point are both of the order $\times 10^{-6}\%$ which suggests that the proposed inverse method can achieve high accuracy estimation.

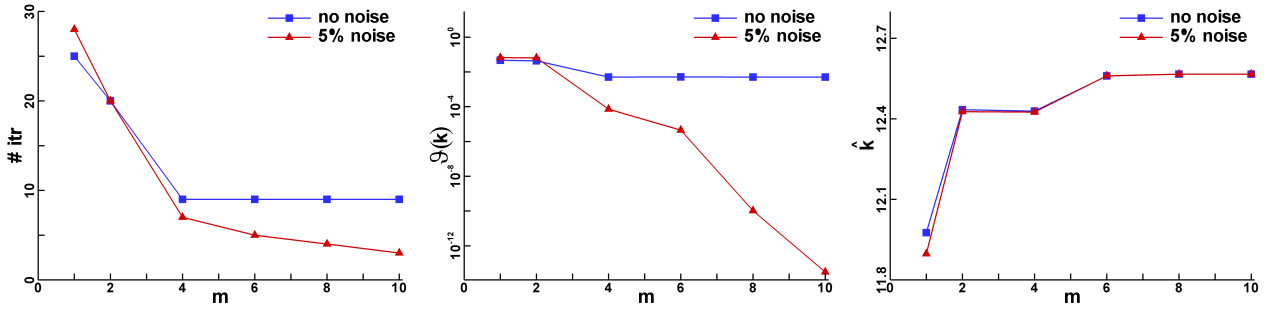

Figure 4.2: Plane wave propagation: Effect of contaminating the data with 5% noise on number of iterations (# itr), minimization function ($\vartheta(k)$) and wavenumber estimate ($\hat{k}$), from left to right.

To further test the robustness of the algorithm, the wave field value at the three considered points is contaminated with a zero-mean white Gaussian noise with the noise-to-signal ratio being 5%. The simulation is also started with the same initial values as in the previous case, namely, $\hat{k}_0 = 30$ and $m_0 = 1$. Figure 4.2 shows a comparison for the number of iterations # itr, minimization function $\vartheta(k)$ and the wavenumber estimate $\hat{k}$ with and without the noise. These quantities are plotted against the number of enrichment functions m. It can be seen in the plot for # itr that the number of iterations needed for the solution to converge is comparable with or without the noise. However, after $m = 4$ the number of iterations stays constant at 9 iterations with the noise while it keeps decreasing without the noise. The minimization function converges to $\vartheta(k) = 0.005$ at $m = 4$ and stays more or less at the same level as the number of enriching plane waves is increased while, again without the noise the function keeps decreasing to $\vartheta(k) = 3.1348 \times 10^{-14}$. Also it can be observed in the plot for wavenumber that the wavenumber estimate improves steadily with the iterations i.e. the estimate does not oscillate. This behaviour seems consistent for clean as well as contaminated data. This also can indicate stability in the proposed algorithm.

Concerning the data contaminated with noise, the proposed algorithm converges again to a very accurate estimate for the wavenumber at $m = 10$ where the stopping tolerances are met. The converged wavenumber and the resulting errors are summarized in Table 4.4. Clearly, the estimated wavenumber is again very close to the exact wavenumber with the error being $\xi_1 = 1.11 \times 10^{-5}\%$ compared to $\xi_1 = 4.78 \times 10^{-6}\%$ from before. However, the estimated value of the wave field at P3 is considerably higher compared to the previous case ($\xi_2 = 2.42\%$ compared to $\xi_2 = 8.1 \times 10^{-6}\%$). This increase in

Table 4.4: Plane wave propagation: Estimation of final errors with contaminated data 5% noise-to-signal.

	Wavenumber	Solution value at P3
Actual	4π=12.5663706	0.96854201 (5% pollution)
Estimate	12.566372	0.99199989
Error	$\xi_1 = 1.1141 \times 10^{-5}\%$	$\xi_2 = 2.42\%$

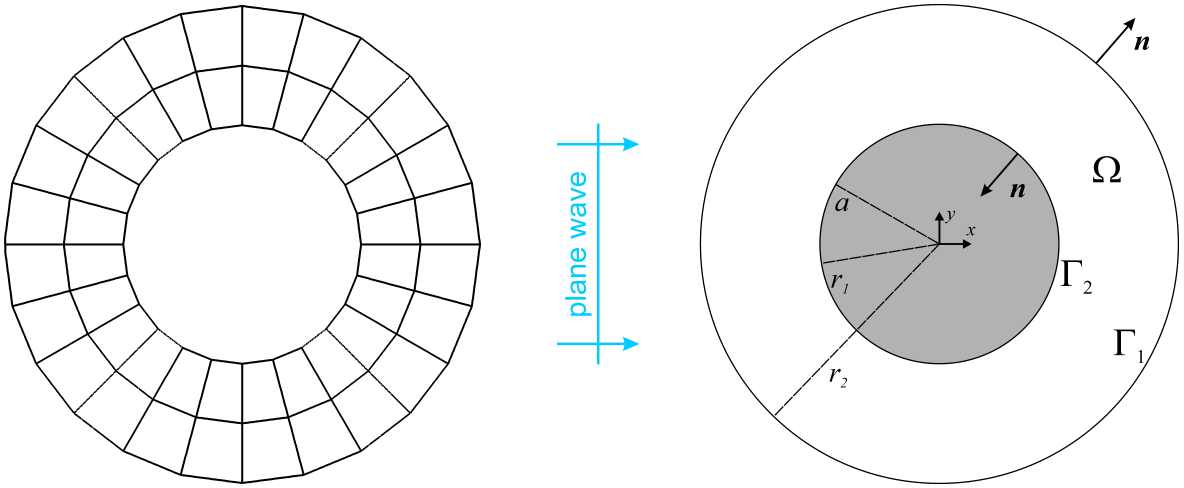

Figure 4.3: Plane wave scattering: Considered mesh (left) and schematic plots of the computational domain Ω, the scatterer and the incident wave (right)

the error is expected considering the 5% noise pollution introduced into the data where the estimated value of the wave field at P3 is much more closer to the uncontaminated data. In general the algorithm shows good robustness for this level of noise.

4.2 Plane wave scattering

In the second test example we consider a plane wave scattering by a circular cylinder. If the cylinder radius is a, then the wave field can be described using the following analytical expression

$$u^s_{\text{ex}} = -\sum_{n=0}^{\infty} \mathrm{i}^n \epsilon_n \frac{J_n{}'(ka)}{H_n{}'(ka)} H_n(kr)\cos(n\theta), \tag{4.2}$$

with r and θ being the polar coordinate. The parameter ϵ_n is 1 when $n = 0$ and is 2 for other values of n while $J_n(kr)$ and $H_n(kr)$ are, respectively, the Hankel function and the Bessel function of the first kind and order n. Figure 4.3 shows schematic plots of the computational domain Ω, the scatterer and the incident wave. The considered computational domain is annular defined by two circular boundaries Γ_1 and Γ_2 with radius equal to $r_1 = 1$ and $r_2 = 2$, respectively. Both boundaries are centred at $(0, 0)$ while a unity radius is considered for the cylinder i.e. $a = 1$. Again we chose to impose the analytical solution of the domain boundaries using the Robin type boundary condition defined by (2.2) where Figure 4.3 shows the considered outward normal $\mathbf{n}$.

To solve the problem the domain is meshed into 4-noded bilinear elements. The mesh is composed of 48 elements and 72 nodes and it is shown in Figure 4.3. The problem is solved for three cases, each case has a different wavenumber, namely, $k = 4\pi, 8\pi$ and 12π. These cases will be referred to as Case 1, Case 2 and Case 3, respectively. The real part of the scattered wave is displayed for these

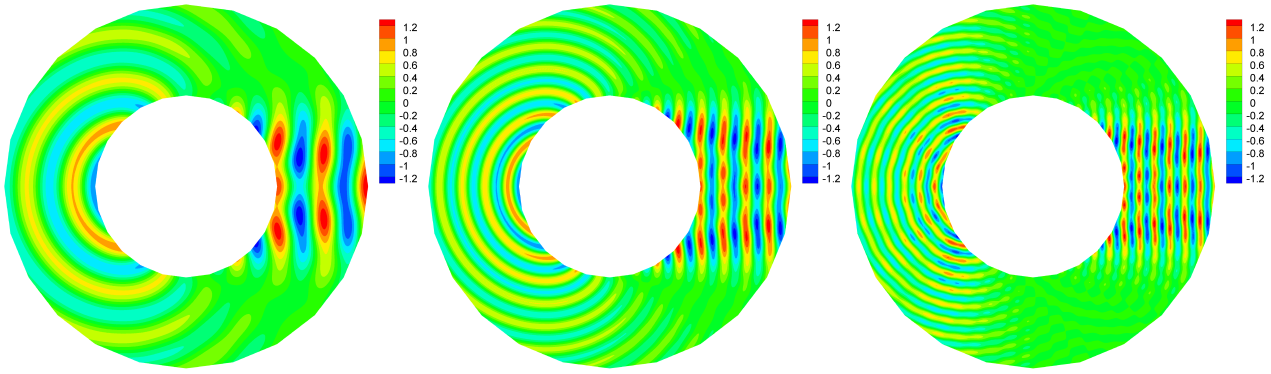

Figure 4.4: Plane wave scattering: Real part of the scattered wave field for $k = 4\pi, 8\pi$ and 12π from left to right.

wavenumbers in Figure 4.4. The stopping tolerances are $\varepsilon_a = \varepsilon_b = 5 \times 10^{-2}$. Again in this example three data points are used, namely, P1(0.5,-0.8660), P2(-0.1857,-1.4077) and P3(1.9319,0.5176) where P1 and P2 are estimation points while P3 is a verification point. Points P1 and P3 are both located on the domain boundaries while P2 is inside the domain. The wave field at these points and for the considered wavenumbers is measured using the analytical expression (4.2). The data at the three points is again considered with and without noise. Using the Gaussian white noise with zero-mean, the data is contaminated with the noise-to-signal ratio being 5%.

In the previous example, to test the convergence of the algorithm with poor initial values, we started with one enrichment function. Obviously using more enrichment functions will improve the PUM approximation. Therefore in this test we start with a relatively high number of enrichment functions. For the wavenumber $k = 4\pi$, the number of enrichment functions is $m_0 = 28$. The number is then increased to $m_0 = 34$ and 44 for $k = 8\pi$ and $k = 12\pi$, respectively. The main reason for this choice, is to avoid listing lengthy tables of convergence, as the higher m will ensure the algorithm convergence without the need to increase the enrichment number in this example. However, it should be stressed that in real-life applications and since the wavenumber is unknown, it will be necessary to make m_0 proportional to the initial estimate of the wavenumber $\hat{k}_0$. For a given mesh a higher value initial guess requires more enrichment functions in order to produce a proper approximation. Furthermore, the algorithm is designed to increase the number of enrichment functions in case the tolerances are not met. Starting from a very high number of enrichment functions and then increase it, may lead to conditioning issues [31]. Therefore it is safer to start from a rather low number of enrichment functions and then increase it. The relation between the wavenumber and the number of enrichment functions are discussed in details in the literature see for example [30, 31].

For Case 1, Case 2 and Case 3 the initial estimates are $\hat{k}_0 = 8, 20$ and 30, respectively. Table 4.5, Table 4.6 and Table 4.7 list the iterations output for each of the considered cases. Final errors associated with all the cases are also summarised in Table 4.8. The iterations converge into an accurate estimate for k in 10, 8 and 7 iterations for Case 1, Case 2 and Case 3, respectively. Tables 4.5 to 4.7 show that a good accuracy is achieved within this relatively small number of iterations. In Case 1 the wavenumber estimate based on the data obtained in P1, leads to a smaller value for the minimization function. Hence, the wavenumber estimate $\hat{k}_{10} = 12.5671$ at P1 is considered as the final output. A similar observation is made for Case 2 where P1 leads to a more accurate estimate while in Case 3 P2 is the more accurate. In fact in Case 3 the more accurate estimate of the wavenumber is also achieved within 7 iterations compared to 13 in P1. The errors in the wavenumber for the Case 1, Case 2 and Case 3 are $\xi_1 = 0.0062\%, 0.0061\%$ and 0.0377%, respectively. The respective errors at the verification point are $\xi_2 = 0.62\%, 0.89\%$ and 4.19%. This is consistent with the previous example where always a larger error is obtained at the verification point compared to the error in the wavenumber.

Table 4.5: Wave scattering: Wavenumber iterations for $k = 4\pi(12.5664)$, $\hat{k}_0 = 8$ and $m = 28$.

# Itr	No noise		Noise (5%)	
	P1	P2	P1	P2
1	8.8000	8.8000	8.8000	8.8000
2	8.4682	12.3086	8.6603	12.5249
3	9.5604	12.6559	10.0329	12.6216
4	10.6393	12.5724	11.7571	12.4634
5	12.5939	12.5802	12.7846	12.4674
6	12.5290	12.5764	12.6284	12.4521
7	12.5644	12.5789	12.5742	12.4245
8	12.5672	12.5751	12.5428	12.3438
9	12.5663	12.5801	12.5443	12.5257
10	12.5671			12.5219
$\hat{k}^q_{opt}$	12.5671*	12.5801	12.5443*	12.5219
$\vartheta(k)$	7.5824×10^{-4}	7.8087×10^{-4}	1.6679×10^{-3}	6.4378×10^{-3}

* the final output.

Table 4.6: Wave scattering: Wavenumber iterations for $k = 8\pi(25.1327)$, $\hat{k}_0 = 20$ and $m = 34$.

# Itr	No noise		Noise (5%)	
	P1	P2	P1	P2
1	22.0000	22.0000	22.0000	22.0000
2	21.1132	24.7914	21.0950	24.7926
3	23.6219	25.1326	23.5787	25.1330
4	24.4334	25.0910	24.3743	25.0912
5	25.0574	25.0927	25.0283	25.0928
6	25.1357		25.1278	
7	25.1380		25.1357	
8	25.1343		25.1366	
$\hat{k}^q_{opt}$	25.1343*	25.0927	25.1366*	25.0928
$\vartheta(k)$	4.5865×10^{-6}	1.5902×10^{-4}	6.1001×10^{-5}	2.9453×10^{-4}

* the final output.

Table 4.7: Wave scattering: Wavenumber iterations for $k = 12\pi(37.6991)$, $\hat{k}_0 = 30$ and $m = 44$.

# Itr	No noise		Noise (5%)	
	P1	P2	P1	P2
1	33.0000	33.0000	33.0000	33.0000
2	29.8412	28.1882	29.8400	28.1623
3	32.7836	37.4518	32.7926	37.2044
4	32.5392	35.5551	32.5596	34.6354
5	34.8063	37.5483	34.8786	37.0903
6	35.9933	37.7129	36.0687	36.9514
7	37.2387	37.7133	37.2849	37.3690
8	37.3567		37.3685	37.6455
9	37.3905		37.3851	37.6917
10	37.3812		37.3846	37.7069
11	37.3393			37.6806
12	37.3906			37.6722
13	37.3870			37.6792
$\hat{k}^q_{opt}$	37.3870	37.7133*	37.3846	37.6792*
$\vartheta(k)$	0.0787	6.7322×10^{-4}	0.0823	8.8225×10^{-3}

* the final output.

Table 4.8: Wave scattering: Solution error for for different wavenumbers.

k	No noise		Noise (5%)	
	ξ_1	ξ_2	ξ_1	ξ_2
4π	0.0062%	0.62%	0.176%	3.35%
8π	0.0061%	0.89%	0.015%	3.75%
12π	0.0377%	4.19%	0.052%	7.26%

It should be pointed out that the wavenumber estimate varied significantly between the starting estimate and the final output. For example in Case 1 we started with $\hat{k}_0 = 8$ while the final output is $\hat{k}_{10} = 12.5671$. In the standard finite element to accommodate such a variation in the wavenumber it is necessary to refine the mesh as a higher wavenumber is estimated. Continuously updating the mesh grid can become a serious computational burden especially if a large number of iterations is needed. In the PUM this was avoided by updating the wavenumber of the enriching plane waves. Furthermore, the same mesh was also retained for all the cases, although the wavenumber was tripled from Case 1 to Case 3. Again this was possible thanks to the enrichment which improves the accuracy of the finite element solution by adding more plane waves rather than refining the mesh.

Concerning contaminated data, Tables 4.5 - 4.7 show that the number of iterations needed for the convergence is in general comparable to that of the clean data. Again here the accuracy of the estimated wavenumber seems to improve consistently with more iterations. The improvement does not show any significant fluctuation in the estimated wavenumber value. This behaviour is consistent for both contaminated and clean data, and confirm a similar observation made in the previous test case. It can be seen in Table 4.8 that the errors are larger for the contaminated data, which is also expected.

5 Conclusions

In this paper, a wavenumber estimation algorithm for the inverse Helmholtz problem is proposed. The iterative algorithm couples the partition of unity method enriched with plane waves to the secant and descent methods. The wavenumber estimation is based on reading the data of the wave field at a number of randomly selected points inside the considered domain or on its boundary. The iterative algorithm works by minimizing a predefined objective function while the convergence is achieved by arriving at predefined tolerances. In general and since the wavenumber is not known, it is important to have the initial number of enrichment functions proportional to the initial wavenumber estimate in order to produce a proper approximation. If the approximation is poor then the algorithm is designed to increase the number of enrichment functions. This increase will happen iteratively until a set of predefined tolerances are met.

To evaluate the algorithm performance we measure the error in the wavenumber or we propose utilizing extra data points. The algorithm is evaluated using two test examples, namely, a wave propagation and a wave scattering problems. The wave field measurements are taken from the analytical solutions of these applications. The results show that the proposed algorithm can achieve high accuracy estimates. Throughout the iterations, the wavenumber estimate seems to improve steadily without significant fluctuation. This behaviour is observed with clean as well as with data contaminated with noise. The robustness of the algorithm is also shown by utilising data contaminated with noise where the algorithm still provided accurate estimates. This also indicate the stability of the algorithm. In practice and if the collected data is incomplete and/or inaccurate it will be necessary to use more data points to have confidence in the wavenumber estimate. Furthermore, the physical knowledge about a problem at hand will help to identify a range where the estimated wavenumber shall fall. This will also provide a useful guide about the accuracy of the wavenumber estimate. The presented results show that using a uniform increase of the enriching basis functions performs well for the cases where the initial guess is higher as well as lower than the exact wavenumber. This was achieved by starting from a minimum number of enrichment functions mainly with one function. Developing an adaptive scheme to relate the increase of the enrichment functions to the increase in the estimated wavenumber would be very useful. However, this will require developing a posteriori error estimate that can evaluate the error in the wavenumber at each iteration. Although the adaptive scheme can reduce the number of iterations but it will also add extra computations related to evaluating the error estimate. This will be looked at in future works.

The literature shows that using an enriched finite element approach can significantly reduce the computational costs of solving forward wave problems. Solving the inverse problem can often involve a large number of iterations, hence, it can be very demanding computationally. This is especially true for high wavenumbers. Therefore, proposing an enriched approach for solving the inverse wave problems can make a major impact on this class of problems. The work presents a first attempt to utilise an enriched finite element approach for the inverse Helmholtz problem. The work also contributes to the inverse Helmholtz problem of identifying the wavenumber where only few resources are available. Extending the proposed method to solve problems in heterogeneous media, can be very useful for identifying subsurface material properties.

Acknowledgements
The authors would like to acknowledge the support provided by Natural Science Foundation of China, No.51775270, and the Fundamental Research Funds for the Central Universities–China, No.NS2017003.

References

[1] MV Klibanov. Two classes of inverse problems for partial differential equations. *Annals of the New York Academy of Sciences*, 661(1):93–111, 1992.

[2] M Tadi, AK Nandakumaran, and SS Sritharan. An inverse problem for Helmholtz equation. *Inverse Problems in Science and Engineering*, 19(6):839–854, 2011.

[3] YA Godin and B Vainberg. A simple method for solving the inverse scattering problem for the difference Helmholtz equation. *Inverse Problems*, 24(2):025007, 2008.

[4] A Karageorghis, D Lesnic, and L Marin. The method of fundamental solutions for the identification of a scatterer with impedance boundary condition in interior inverse acoustic scattering. *Engineering Analysis with Boundary Elements*, 92:218–224, 2018.

[5] A Karageorghis, D Lesnic, and L Marin. The MFS for the identification of a sound-soft interior acoustic scatterer. *Engineering Analysis with Boundary Elements*, 83:107–112, 2017.

[6] A El Badia and A El Hajj. Identification of dislocations in materials from boundary measurements. *SIAM Journal on Applied Mathematics*, 73(1):84–103, 2013.

[7] A El Badia and T Nara. An inverse source problem for Helmholtz's equation from the Cauchy data with a single wave number. *Inverse Problems*, 27(10):105001, 2011.

[8] T Kolokolnikov and AE Lindsay. Recovering multiple small inclusions in a three-dimensional domain using a single measurement. *Inverse Problems in Science and Engineering*, 23(3):377–388, 2015.

[9] B Jin and Y Zheng. A meshless method for some inverse problems associated with the Helmholtz equation. *Computer Methods in Applied Mechanics and Engineering*, 195(19-22):2270–2288, 2006.

[10] B Jin and W Rundell. A tutorial on inverse problems for anomalous diffusion processes. *Inverse Problems*, 31(3):035003, 2015.

[11] G Bao, P Li, and Y Zhao. Stability in the inverse source problem for elastic and electromagnetic waves with multi-frequencies. *arXiv preprint arXiv:1703.03890*, 2017.

[12] A El Badia and A El Hajj. Stability estimates for an inverse source problem of Helmholtz's equation from single Cauchy data at a fixed frequency. *Inverse Problems*, 29(12):125008, 2013.

[13] G Bao, J Lin, and F Triki. Numerical solution of the inverse source problem for the Helmholtz equation with multiple frequency data. *Contemporary Mathematics*, 548:45–60, 2011.

[14] D Zhang and Y Guo. Fourier method for solving the multi-frequency inverse source problem for the Helmholtz equation. *Inverse Problems*, 31(3):035007, 2015.

[15] X Wang, Y Guo, D Zhang, and H Liu. Fourier method for recovering acoustic sources from multi-frequency far-field data. *Inverse Problems*, 33(3):035001, 2017.

[16] G Wang, F Ma, Y Guo, and J Li. Solving the multi-frequency electromagnetic inverse source problem by the Fourier method. *arXiv preprint arXiv:1708.00673*, 2017.

[17] D Colton and R Kress. *Inverse acoustic and electromagnetic scattering theory*, volume 93. Springer Science & Business Media, 2012.

[18] Y Guo, P Monk, and D Colton. Toward a time domain approach to the linear sampling method. *Inverse Problems*, 29(9):095016, 2013.

[19] YA Gryazin, MV Klibanov, and TR Lucas. Two numerical methods for an inverse problem for the 2-D Helmholtz equation. *Journal of Computational Physics*, 184(1):122–148, 2003.

[20] ET Chung, Y Efendiev, B Jin, WT Leung, and M Vasilyeva. Generalized multiscale inversion for heterogeneous problems. *arXiv preprint arXiv:1707.08194*, 2017.

[21] JC Nédélec. *Acoustic and electromagnetic equations: Integral representations for harmonic problems*, volume 144. Springer Science & Business Media, 2001.

[22] MA Sumbatyan and A Scalia. *Equations of mathematical diffraction theory*. CRC Press, 2004.

[23] B Pluymers. *Wave based modelling methods for steady-state vibro-acoustics. KULeuven, division PMA*. PhD thesis, PhD. thesis 2006D04, http://www. mech. kuleuven. be/mod/wbm/phd_dissertations, 2006.

[24] A Van Hirtum. Quasi-analytical solution of two-dimensional Helmholtz equation. *Applied Mathematical Modelling*, 47:96–102, 2017.

[25] HH Qin and F Cakoni. Nonlinear integral equations for shape reconstruction in the inverse interior scattering problem. *Inverse Problems*, 27(3):035005, 2011.

[26] F Ihlenburg and I Babuška. Finite element solution of the Helmholtz equation with high wave number part I: The h-version of the FEM. *Computers & Mathematics with Applications*, 30(9):9–37, 1995.

[27] A Deraemaeker, I Babuška, and P Bouillard. Dispersion and pollution of the FEM solution for the Helmholtz equation in one, two and three dimensions. *International Journal for Numerical Methods in Engineering*, 46(4):471–499, 1999.

[28] K Christodoulou, O Laghrouche, MS Mohamed, and J Trevelyan. High-order finite elements for the solution of Helmholtz problems. *Computers & Structures*, 191:129–139, 2017.

[29] JM Melenk and I Babuška. The partition of unity finite element method: Basic theory and applications. *Computer Methods in Applied Mechanics and Engineering*, 139:289–314, 1996.

[30] O Laghrouche, P Bettess, E Perrey-Debain, and J Trevelyan. Wave interpolation finite elements for Helmholtz problems with jumps in the wave speed. *Computer Methods in Applied Mechanics and Engineering*, 194(2):367–381, 2005.

[31] MS Mohamed, O Laghrouche, and A El-Kacimi. Some numerical aspects of the PUFEM for efficient solution of 2D Helmholtz problems. *Computers & Structures*, 88(23):1484–1491, 2010.

[32] O Laghrouche and MS Mohamed. Locally enriched finite elements for the Helmholtz equation in two dimensions. *Computers & Structures*, 88:1469–1473, 2010.

[33] JD Chazot, B Nennig, and E Perrey-Debain. Performances of the partition of unity finite element method for the analysis of two-dimensional interior sound fields with absorbing materials. *Journal of Sound and Vibration*, 332(8):1918–1929, 2013.

[34] MS Mahmood, O Laghrouche, J Trevelyan, and A El Kacimi. Implementation and computational aspects of a 3D elastic wave modelling by PUFEM. *Applied Mathematical Modelling*, 49:568–586, 2017.

[35] M Drolia, MS Mohamed, O Laghrouche, M Seaid, and J Trevelyan. Enriched finite elements for initial-value problem of transverse electromagnetic waves in time domain. *Computers & Structures*, 182:354–367, 2017.

[36] R Adriano, WG Facco, and EJ Silva. A modified plane wave enrichment to solve 2-D electromagnetic problems using the generalized finite-element method. *IEEE Transactions on Magnetics*, 51(3):1–4, 2015.

[37] GC Diwan, MS Mohamed, M Seaid, J Trevelyan, and O Laghrouche. Mixed enrichment for the finite element method in heterogeneous media. *International Journal for Numerical Methods in Engineering*, 101(1):54–78, 2015.

[38] JD Chazot, E Perrey-Debain, and B Nennig. The partition of unity finite element method for the simulation of waves in air and poroelastic media. *The Journal of the Acoustical Society of America*, 135(2):724–733, 2014.

[39] MS Mohamed, M Seaid, J Trevelyan, and O Laghrouche. A partition of unity FEM for time-dependent diffusion problems using multiple enrichment functions. *International Journal for Numerical Methods in Engineering*, 93:245–265, 2013.

[40] P O'Hara, CA Duarte, and T Eason. Transient analysis of sharp thermal gradients using coarse finite element meshes. *Computer Methods in Applied Mechanics and Engineering*, 200:812–829, 2011.

[41] MS Mohamed, M Seaid, J Trevelyan, and O Laghrouche. Time-independent hybrid enrichment for finite element solution of transient conduction-radiation in diffusive grey media. *Journal of Computational Physics*, 251:81–101, 2013.

[42] H Li and CA Duarte. A two-scale generalized finite element method for parallel simulations of spot welds in large structures. *Computer Methods in Applied Mechanics and Engineering*, 2018.

[43] R Tezaur, I Kalashnikova, and C Farhat. The discontinuous enrichment method for medium-frequency Helmholtz problems with a spatially variable wavenumber. *Computer Methods in Applied Mechanics and Engineering*, 268:126–140, 2014.

[44] C Farhat, I Harari, and LP Franca. The discontinuous enrichment method. *Computer Methods in Applied Mechanics and Engineering*, 190(48):6455–6479, 2001.

[45] T Luostari, T Huttunen, and P Monk. Improvements for the ultra weak variational formulation. *International Journal for Numerical Methods in Engineering*, 94(6):598–624, 2013.

[46] CJ Howarth, PN Childs, and A Moiola. Implementation of an interior point source in the ultra weak variational formulation through source extraction. *Journal of Computational and Applied Mathematics*, 271:295–306, 2014.

[47] NC Nguyen, J Peraire, F Reitich, and B Cockburn. A phase-based hybridizable discontinuous Galerkin method for the numerical solution of the Helmholtz equation. *Journal of Computational Physics*, 290:318–335, 2015.

[48] R Dias, EGD do Carmo, WJ Mansur, and CSG Monteiro. A discontinuous Petrov–Galerkin (DPG) formulation for the FEM applied to the Helmholtz equation for high wavenumbers. *Journal of the Brazilian Society of Mechanical Sciences and Engineering*, 39(5):1529–1544, 2017.

[49] S Kapita and P Monk. A plane wave discontinuous Galerkin method with a Dirichlet-to-Neumann boundary condition for the scattering problem in acoustics. *Journal of Computational and Applied Mathematics*, 327:208–225, 2018.

[50] R Hiptmair, A Moiola, and I Perugia. A survey of Trefftz methods for the Helmholtz equation. In *Building bridges: connections and challenges in modern approaches to numerical partial differential equations*, pages 237–278. Springer, 2016.

[51] CT Kelley. *Iterative methods for optimization*. SIAM, 1999.

[52] MS Mohamed, O Laghrouche, and J Trevelyan. A q-adaptive partition of unity finite element method for the solution of the 2D Helmholtz equation. In *IOP Conference Series: Materials Science and Engineering*, volume 10, page 012148. IOP Publishing, 2010.